

Integrative approaches generate insights into the architecture of non-syndromic cleft lip with or without cleft palate

Julia Welzenbach,¹ Nigel L. Hammond,² Miloš Nikolić,³ Frederic Thieme,¹ Nina Ishorst,¹ Elizabeth J. Leslie,⁴ Seth M. Weinberg,^{5,6} Terri H. Beaty,⁷ Mary L. Marazita,^{5,6,8} Elisabeth Mangold,¹ Michael Knapp,⁹ Justin Cotney,^{10,11} Alvaro Rada-Iglesias,^{3,12,13} Michael J. Dixon,² and Kerstin U. Ludwig^{1,*}

Summary

Non-syndromic cleft lip with or without cleft palate (nsCL/P) is a common congenital facial malformation with a multifactorial etiology. Genome-wide association studies (GWASs) have identified multiple genetic risk loci. However, functional interpretation of these loci is hampered by the underrepresentation in public resources of systematic functional maps representative of human embryonic facial development. To generate novel insights into the etiology of nsCL/P, we leveraged published GWAS data on nsCL/P as well as available chromatin modification and expression data on mid-facial development. Our analyses identified five novel risk loci, prioritized candidate target genes within associated regions, and highlighted distinct pathways. Furthermore, the results suggest the presence of distinct regulatory effects of nsCL/P risk variants throughout mid-facial development and shed light on its regulatory architecture. Our integrated data provide a platform to advance hypothesis-driven molecular investigations of nsCL/P and other human facial defects.

Introduction

Current research into the etiology of common disorders is focused on the identification of genetic susceptibility factors and the manner in which these risk variants interfere with biological function. Over the past decade, genome-wide association studies (GWASs) of common disorders have identified numerous risk loci. However, success in the translation of statistical associations from GWASs into functional mechanisms is only a very recent achievement.^{1–6} A major driver of these advances has been the availability of large-scale genetic data and the systematic integration of genetic, transcriptional, epigenetic, and other -omics datasets from disease-relevant cell types and tissues.⁷

Facial disorders rank among the most common birth defects worldwide and represent a substantial burden for affected individuals, their families, and healthcare systems.^{8,9} The most frequent facial disorder is non-syndromic cleft lip with or without cleft palate (nsCL/P). This condition has a global incidence of ~1 in 1,000 live births⁹ and is characterized by a multifactorial etiology that includes an overall genetic contribution of around

90%.^{9–11} On an epidemiological level, nsCL/P is associated with an increased risk for adverse health outcomes.¹² However, this observation remains largely unexplained at both the clinical and molecular levels. To date, GWASs and other systematic approaches have identified at least 40 nsCL/P risk loci,^{13–28} which explain up to 30% of the estimated heritability in European populations.²¹ Despite these successes, functional dissection of the associated regions has been limited to only a few loci.^{29–32} This is mainly attributable to the systematic underrepresentation of embryonic facial data in public resources such as ENCODE,³³ Roadmap Epigenome,³⁴ and GTEx.³⁵ To overcome this limitation, researchers have recently profiled multiple chromatin modifications in cell types and tissues of relevance to individual time points of mid-facial development, a process that is largely completed by week 10 of gestation (Figure 1A). These cell types and tissues include early human neural crest cells (hNCCs),³⁷ lineage-specified human cranial NCCs (cNCCs),³⁸ and embryonic mid-facial tissue samples encompassing the time period 4.5–10 weeks post-conception (craniofacial tissue [CT]; days 32–56 of gestation).³⁹ Previous studies have demonstrated a significant enrichment of nsCL/P-GWAS

¹Institute of Human Genetics, University Hospital Bonn, Medical Faculty, Venusberg-Campus 1, 53127 Bonn, Germany; ²Faculty of Biology, Medicine, and Health, Manchester Academic Health Sciences Centre, University of Manchester, Manchester M13 9PT, UK; ³Center for Molecular Medicine Cologne (CMCC), University of Cologne, Cologne, Germany; ⁴Department of Human Genetics, School of Medicine, Emory University, Atlanta, GA, USA; ⁵Center for Craniofacial and Dental Genetics, Department of Oral Biology, School of Dental Medicine, University of Pittsburgh, Pittsburgh, PA, USA; ⁶Department of Human Genetics, Graduate School of Public Health, University of Pittsburgh, Pittsburgh, PA, USA; ⁷Department of Epidemiology, Bloomberg School of Public Health, Johns Hopkins University, Baltimore, MD, USA; ⁸Department of Psychiatry and Clinical and Translational Science Institute, School of Medicine, University of Pittsburgh, Pittsburgh, PA 15260, USA; ⁹Institute of Medical Biometry, Informatics, and Epidemiology, University Hospital Bonn, Bonn, Germany; ¹⁰Department of Genetics and Genome Sciences, UConn Health, Farmington, CT, USA; ¹¹Institute for Systems Genomics, University of Connecticut, Storrs, CT, USA; ¹²Cluster of Excellence Cellular Stress Responses in Aging-Associated Diseases (CECAD), University of Cologne, Cologne, Germany; ¹³Institute of Biomedicine and Biotechnology of Cantabria (IBBT), University of Cantabria, Cantabria, Spain

*Correspondence: kerstin.ludwig@uni-bonn.de

<https://doi.org/10.1016/j.xhgg.2021.100038>

© 2021 The Authors. This is an open access article under the CC BY-NC-ND license (<http://creativecommons.org/licenses/by-nc-nd/4.0/>).



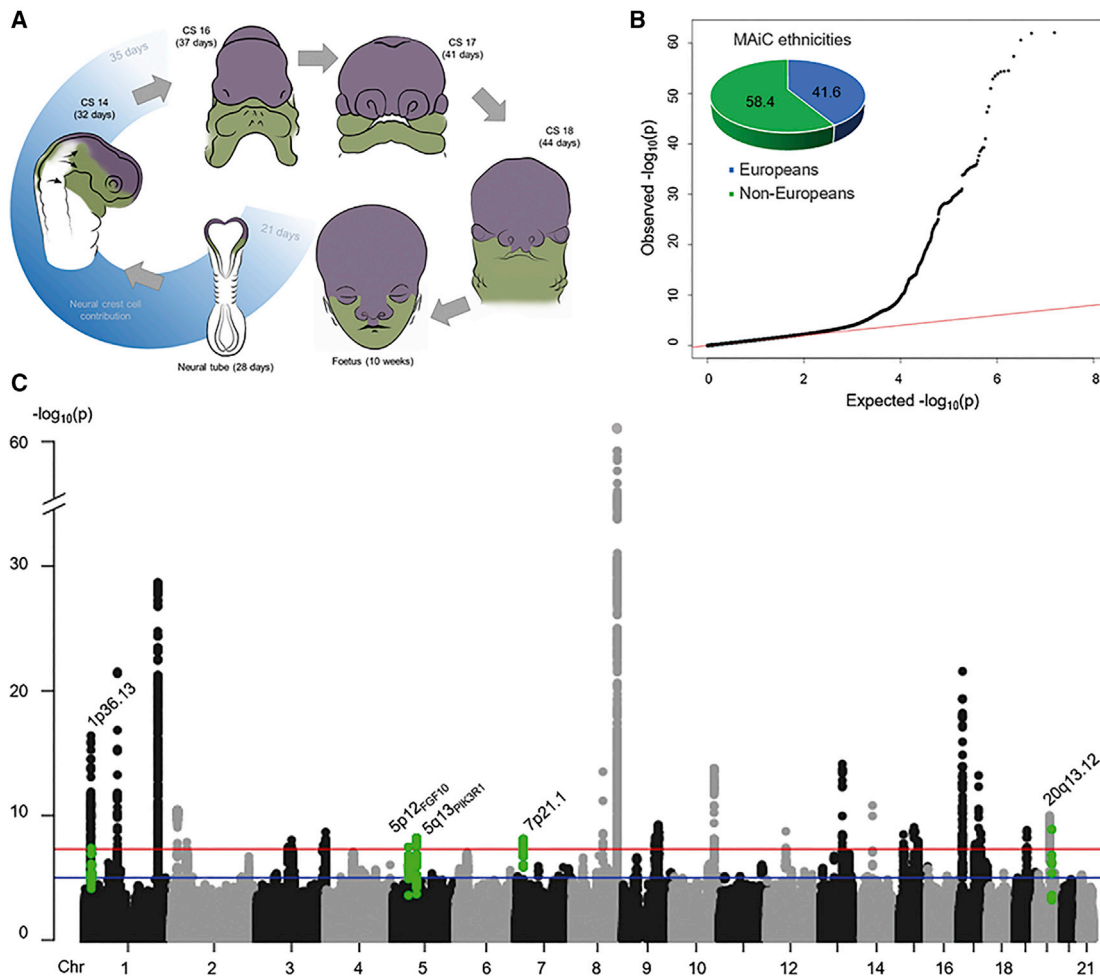


Figure 1. Human facial development and results of meta-analysis in clefting (MAiC)

(A) Schematic representation. The first phase of facial development (blue shading) is characterized by a substantial contribution of neural crest cells (NCCs): In early embryogenesis, NCCs arise in the ectoderm, undergo epithelial-to-mesenchymal transition, and begin to migrate from the dorsal neural tube. An NCC fraction (i.e., cranial NCCs) contribute to the pre-swellings of the face and populate the future frontonasal prominence as well as the first (purple) and second (green) pharyngeal arches.³⁶ Subsequently, NCC-derived cells fuse to form those human facial structures that are finalized by the 10th week of embryogenesis.

(B) MAiC quantile-quantile plot. Observed statistical associations for non-syndromic cleft lip with/without cleft palate (nsCL/P) are plotted against the association statistics expected under the null hypothesis of no association. The contribution of different ethnicities in MAiC is shown using a pie chart.

(C) MAiC Manhattan plot. MAiC $-\log_{10}(p)$ association results are plotted along their chromosomal distribution. Blue and red lines indicate suggestive ($p < 10^{-5}$) and genome-wide ($p < 5 \times 10^{-8}$) significance, respectively. The lowest p value was observed for rs55658222 ($p = 8.69 \times 10^{-63}$), located at 8q24.²⁷ Novel risk loci are highlighted in green (lead variant plus variants in linkage disequilibrium [LD] [$r^2 \geq 0.6$]). Gene names in subscript discriminate novel risk loci in situations where the respective chromosomal band is already listed among the 40 risk loci.

variants in active chromatin regions from both hNCCs and CT.^{21,39} To date, however, the fact that these datasets have been generated from differing sources has precluded the integrative analyses required for a comprehensive assessment of variant function at different time points of mid-facial development.

To generate novel insights into the etiology of nsCL/P, the present study leveraged both existing GWAS data on nsCL/P and epigenetic data on mid-facial development. The specific aims of the study were threefold (Figure S1). First, we generated one of the largest genome-wide genetic datasets for nsCL/P to date by combining three GWASs, which collectively encompassed European, Asian, and

Latin American ethnicities. Using this resource, which we term MAiC (meta-analysis in clefting), we confirmed the vast majority of established risk regions and detected five novel loci (the strategy for identification of novel risk loci is described in the Supplemental Material and methods). To shed light on potential etiological overlaps between nsCL/P and other phenotypes, we then cross-referenced the lead variants at nsCL/P risk loci with GWAS data on >3,000 common traits and identified a set of loci with pleiotropic effects. Second, we compiled a comprehensive epigenetic map of mid-facial development through joint analyses of available data from hNCCs, cNCCs, and CT. This resource of chromatin segments

across mid-facial development serves as a platform for the interpretation of genetic findings for facial disorders and traits. Finally, we aimed to generate systematic insights into nsCL/P biology by combining MAiC and epigenetic data and then adding additional layers on gene expression in NCCs and global and local three-dimensional (3D) genomic interactions (i.e., topologically associated domains [TADs],⁴⁰ promoter-capture HiC [pChI-C]⁴¹). This approach revealed tissue- and time-point-specific regulatory effects at GWAS risk loci, prioritized candidate target genes, and highlighted distinct pathways. To our knowledge, the present report is the first to describe the systematic integration of large-scale summary statistics in nsCL/P and data on the *cis*-regulatory landscape across several stages of human mid-facial development.

Material and methods

GWAS meta-analysis MAiC

Cohort description

The meta-analysis included data from three previously published individual GWASs on nsCL/P (Bonn case-control GWAS cohort,¹⁸ GENEVA trio cohort,²⁰ POFC GWAS cohort;¹⁷ Table S1). We included all nsCL/P summary statistics that were publicly accessible until June 2018. Data from the Bonn cohort were available in-house, while both the GENEVA (dbGaP: phs000094) and POFC (dbGaP: phs000774) datasets were downloaded from dbGaP upon approved data access, respectively. Previously conducted meta-analyses included combinations of two of these studies (Bonn and GENEVA GWAS cohort in Ludwig et al., 2012¹⁹ [genotyped variants] and 2017²¹ [imputed variants], GENEVA and POFC in Leslie et al.²⁶). In the present study we combined the three GWAS cohorts to generate the largest nsCL/P meta-analysis to date. In accordance with previous studies,^{19,21,26} two meta-analyses were performed: (1) using all individuals with diverse population backgrounds (to increase statistical power by maximizing sample size; in the following termed as MAiC), and (2) using the European datasets only (MAiC_{Euro}, to reduce genetic heterogeneity based on population differences). Data quality control (QC) included the detection and removal of overlapping individuals, confirmation of ethnicity, and data re-analysis. We call this new dataset MAiC to provide a clear distinction from the previous individual studies and meta-analyses of sub-cohorts. Further details in cohort description and data QC can be found in the [Supplemental information](#).

Statistical analyses

Statistical analyses were performed separately for case-control cohorts and case-parent trios, respectively. Imputed data were taken as provided by dbGaP (POFC) or generated as previously described (for Bonn and GENEVA),²¹ respectively, and best-guess genotypes were assigned based on *a posteriori* genotype probabilities of ≥ 0.6 . In the case-control cohorts, GWAS was performed using logistic regression performed with SNPTEST and -method expected, by incorporating five (Bonn and GENEVA cohorts) and 18 (POFC cohort) dimensions of the multi-dimensional-scaling coordinates,⁴² respectively. For the case-parent trios, a transmission disequilibrium test (TDT) was performed on the best-guess genotypes.⁴³ After data cleaning procedures ([Supplemental information](#)), we meta-analyzed the GWAS data of all four sub-cohorts (Bonn case-control, GENEVA case-parent trios, POFC case-control, and POFC case-parent trios) using METAL.⁴⁴

The final MAiC dataset (case-control plus case-parent trios) contained 6,825 individuals (including 3,946 affected; MAiC_{Euro}: 3,568 individuals including 1,517 affected; Table S1). The maximum genomic inflation factor was 1.051 (GENEVA) and 1.056 (POFC case-control) for MAiC and MAiC_{Euro}, respectively. All functional downstream analyses are based on MAiC because of largely increased statistical power. To estimate the single-nucleotide polymorphism (SNP)-based heritability (h^2) for nsCL/P on the liability scale, we generated a European case-control-only dataset (Bonn, POFC, totaling 532 cases and 2,051 controls; Table S1) and performed linkage disequilibrium (LD) score regression as implemented in ldsr.⁴⁵ Sample and population prevalence were set to 0.21 and 0.001, respectively.

Gene-based and pathway analyses

Gene-based analyses in MAiC and MAiC_{Euro} were performed using MAGMA⁴⁶ (v.1.06), implemented in FUMA. The input SNPs of MAiC were mapped to 17,911 protein-coding genes based to a distance of 0 kb upstream/downstream of the genes, resulting in threshold of test-wide significance of $p = 2.79 \times 10^{-6}$ (i.e., 0.05/17,911). To annotate known and novel nsCL/P risk loci in biological context, we investigated common expression patterns of the GWAS_{TAD} genes and their molecular functions (gene ontology [GO] terms, Kyoto Encyclopedia of Genes and Genomes (KEGG) pathways) using FUMAs “GENE2FUNC” tool in (1) all GWAS_{TAD} genes, and (2) a subset of GWAS_{TAD} genes expressed in NCCs. This approach allows us to pinpoint risk loci or genes that are functionally involved in the same pathways or molecular processes and might be useful for gene prioritization.

Analysis of pleiotropic effects using the GWAS ATLAS

For each of the 45 lead SNPs in MAiC, association signals from large-scale genetic studies (including p value, effect size, and effect direction) were retrieved from the GWAS ATLAS.⁴⁷ At time of analysis (November 2019), the database comprised 4,756 GWASs on 3,302 unique traits. Notably, the unique traits are split into 28 domains, of which we combined two (environment, activities) into one domain to reduce redundancy. All significant SNP-trait associations at $p < 0.05$ were considered, and this number was corrected for the number of GWASs and loci in the analysis.

Epigenetic datasets for mid-facial development

Identification of datasets relevant to mid-facial development

Human cell-type- and developmental-stage-specific data for mid-facial development are underrepresented (or not represented at all) in large consortia data such as ENCODE.³³ However, available data in the Gene Expression Omnibus (GEO) covered mid-facial development from (1) early stages (hNCCs,³⁷ accessed through GEO: GSE28874), (2) differentiated human cNCCs³⁸ (accessed through GEO: GSE70751), and (3) embryonic craniofacial human tissue of different Carnegie stages (CS) (accessed through GEO: GSE97752).³⁹ In each of these datasets, analyses of chromatin modifications were performed using chromatin immunoprecipitation followed by sequencing (chromatin immunoprecipitation sequencing [ChIP-seq]) or are available as imputed datasets. Detailed information including antibodies used in these studies is shown in Table S3 and in the [Supplemental information](#). For hNCCs and cNCCs, ChIP-seq had been performed for chromatin modifications H3K27ac, H3K4me1, H3K4me3, and H3K27me3. In CT, for samples of CS13–CS17, ChIP-seq was performed for H3K27ac, H3K4me1, H3K4me3, H3K27me3, and H3K36me3 (Table S4), and data for H3K9me3 were imputed. For CS20 and

10 wpc, H3K27ac3 ChIP-seq data were experimentally derived; all other marks were imputed (Table S3).

Data processing

For hNCCs and cNCCs, raw data were available in fastq format. A description of data QC is given in Rada-Iglesias et al.³⁷ and Prescott et al.,³⁸ respectively. ChIP-seq data from craniofacial data in Wilderman et al.³⁹ comprise processed formats, including imputed signals, peaks, and segmentation data. In order to ensure comparability among the three data sources, computational processing of ChIP-seq data as published in Wilderman et al.³⁹ (QC, alignment, peak calling, epigenetic imputation, chromatin segmentation) was adopted to the hNCC/cNCC bioinformatics pipeline, as described in the Supplemental information and Table S5.

Chromatin imputation and segmentation

To obtain uniform datasets, chromatin imputation followed by chromatin state segmentation was performed. First, H3K9me3 and H3K36me3 marks in hNCCs/cNCCs were imputed using ChromImpute (v.1.0.1),⁴⁸ based on 127 cell types from the Roadmap Epigenome Project.³⁴

Imputed hNCC/cNCC signal files for each individual chromosome and each chromatin mark were binarized, and segmentation was performed using the core+K27ac 18-state chromatin model provided by Roadmap with ChromHMM⁴⁹ to predict 18 chromatin states. Because of the low number of chromatin marks measured in the NCC samples, epigenetic imputation issues, and the higher risk of batch effect between hNCCs, cNCCs, and CT, we adopted a robust strategy and condensed the 18 generated states into eight states, based on Roadmap definition: three active states (transcription starting sites [TSS], transcribed sites, and enhancers [Enh]), one bivalent state (Poised Enh/bivalent TSS), three repressed states (Heterochromatin, Repressed PolyComb sites, Zinc finger genes/Repeats), and one quiescent state (Quies). Potential batch effects were analyzed using principal-component analysis (PCA) and hierarchical clustering of Pearson correlation coefficients.

Other datasets

To identify genome-wide regulatory genomic units, we used TADs from human embryonic stem cells (hESCs) (H1 cell line) as provided by the Ren Lab.⁴⁰ Protein-coding genes were extracted from UCSC genome browser (hg19) and were mapped to TADs using positional information. TADs containing an nsCL/P risk locus were defined as GWAS_{TAD} region. Based on previous evidence for complex regulatory interactions within one TAD, we considered all genes from the GWAS_{TAD} region as potential candidate genes for downstream effects of the associated variants in the $r^2 \geq 0.6$ region. Expression data from NCCs (two replicates of day11hNCC [GEO: GSE121428] and three replicates of passage2hNCC [GEO: GSE108521]) were retrieved from Lausch et al. (GEO: GSE108522).⁵⁰ For the comparison of genes in TADs of nsCL/P risk loci and genes expressed in NCCs, we used the average RNA-seq Fragments Per Kilobase Million (FPKM) across five samples. To identify functional links between different regulatory features (e.g., DNA-DNA interactions of enhancers and TSS) at specific risk loci, we accessed pChIP-C *cis*-interaction data collected in hESCs (GEO: GSE86821).⁴¹

Translation of genetic associations into tissue- and time-point-specific regulatory effects at a systematic level

Enrichment analyses using GREGOR

Based on chromatin segments obtained from hNCCs, cNCCs, and CT, we used GREGOR (Genomic Regulatory Elements and GWAS Overlap Algorithm)⁵¹ to evaluate the enrichment of significant

SNPs from the MAiC data in the available regulatory features (i.e., eight predicted chromatin states). As described in the Supplemental information, a set of samples from the Roadmap Epigenomics project (comprising both fetal and adult tissue samples) was selected as an independent dataset for comparison. As input, we used MAiC nsCL/P variants with $p \leq 0.001$ without additional variants in LD ($n = 22,999$); this threshold was selected to balance between adequate statistical power and true-positive association signals.

CT- and NCC-specific active chromatin sites

To examine specific effects in either NCCs or CT, we filtered in the chromatin segmentation datasets for active chromatin sites (TSS, Enhancer or transcribed sites) in NCCs that are repressed/quiet (Quiescent, Biv_TSS_pois_enh, ReprPC, Heterochromatin) in CT and vice versa. For robust observations, we only trust in a chromatin state if it is present in both NCC samples (hNCCs, cNCCs) or in five of the six CT (CS13, CS14, CS15, CS17, CS20, 10wpc) samples. To account for biases in length associated with batch effects, active sites were only retained if they had a distance of ≥ 500 bp to any chromatin segment of opposite activity status in the other cell system/tissue. In the following, we combined the specific active chromatin sites with MAiC associations and TAD data to filter for TADs with high density of strong associated genetic variants ($p_{\text{MAiC}} \leq 5 \times 10^{-5}$) in specific active chromatin sites at new and known nsCL/P GWAS risk loci.

Characterization of nsCL/P risk variants and candidate gene prioritization in context of epigenetic mid-facial timeline

For comprehensive insights in regulatory mechanisms at nsCL/P risk loci, we finally integrated all available genetic and functional data (MAiC associations, GWAS_{TAD}- and $r^2 \geq 0.6$ -region boundaries, NCC- and CT-specific active chromatin sites, chromatin segmentation tracks, and pChIP-C *cis* interactions). Based on this approach, we attempt to prioritize genetic variants with regulatory effect and potential downstream target genes and to detect relevant regulatory elements specific for the early (hNCC/cNCC) or later mid-facial development (CT).

Results

MAiC identifies five novel risk loci

The MAiC dataset was generated by combining GWAS data from three previous studies (Bonn,¹⁸ GENEVA,²⁴ POFC¹⁷), following the exclusion of overlapping individuals and extensive QC. The final dataset comprised 1,247 nsCL/P cases, 2,879 controls, and 2,699 case-parent trios of multiple ethnicities, and ~ 7.74 million SNPs. The p value distribution was consistent with a multifactorial inheritance (Figure 1B; $\lambda = 1.07$). A set of 1,375 SNPs achieved genome-wide significance ($p < 5 \times 10^{-8}$; Figure 1C). Analysis of established nsCL/P risk loci in MAiC revealed genome-wide significant SNPs at 25 of the 40 regions. These 25 regions comprised 22/26 loci that were previously identified in GWASs based on largely European samples and 3/14 loci reported in individuals from the Chinese population.^{13,22} At all other nsCL/P risk loci ($n = 15$), nominal significance ($p < 0.05$) was observed for individual

variants that were in strong LD ($D' > 0.8$) with the respective lead SNP (Table S2).

Importantly, the MAiC analyses also identified five novel risk loci ($p < 5 \times 10^{-8}$), thus increasing the number of identified nsCL/P GWAS risk loci to 45. These novel loci were located at chromosomes 1p36.13 (sentinel variant rs34746930), 5p12_{FGF10} (rs60107710), 5q13.1_{PIK3R1} (rs6449957), 7p21.1 (rs62453366), and 20q13.12 (rs3091552; Table 1). Consistent with previous findings on risk variants for nsCL/P and other complex traits,²⁹ these lead variants map to non-coding regions that are adjacent to candidate genes with functions during facial development, such as *CAPZB*⁵² and *NBL1*⁵³ (both at 1p36) and *EYA2*⁵⁴ (at 20q13; Supplemental text; Figures S2–S6). To identify population-specific effects, a sub-analysis was performed in individuals from Central Europe (MAiC_{Euro}; $n = 562$ cases, 2,051 controls, and 955 case-parent trios). No additional risk loci were identified at the level of genome-wide significance (Figure S7; Table S2). Using this European case-control cohort and LD score regression,⁴⁵ SNP-based heritability was estimated as $h^2 = 28\% \pm 0.1\%$. This confirmed previous heritability estimates obtained using the Bonn cohort only.²¹

Gene-based analyses suggest nsCL/P candidate genes outside of GWAS risk loci

Using MAiC summary statistics and MAGMA,⁴⁶ gene-based analyses yielded 1,357 genes with nominal significance ($p < 0.05$; Figure S8A). A total of 25 genes reached test-wide significance ($p < 2.79 \times 10^{-6}$; Table S6). Of these, 23 map to known GWAS risk loci. For some of these 23 genes, functional evidence strongly supports their involvement in nsCL/P (e.g., *IRF6*,⁵⁵ *TP63*⁵⁶). This analysis also suggested novel candidate genes at GWAS risk loci, such as *ARID3B*. In mice, the gene *Arid3b* is expressed in cranial mesenchyme structures and has been shown to interact with *Mycn*, which is encoded by a strong candidate gene at another nsCL/P risk locus.^{57,58} Two genes with a significant burden of common variants mapped outside all known GWAS risk loci. These genes, *BTN3A3* ($p_{\text{gene}} = 6.96 \times 10^{-7}$) and *BTN3A1* ($p_{\text{gene}} = 2.44 \times 10^{-6}$; Figure S9A), are both located at chromosome 6p22.2, and previous research found that *BTN3A3* showed differential expression in the lip tissue of CL/P phenotypic subgroups.⁵⁹ In MAiC_{Euro}, the gene-based analysis revealed 11 genes with test-wide significance (Figure S8B; Table S7), including three novel candidate genes (*LIMCH1*, *MSX2*, and *STRA13*; Figures S9B–S9D). Overall, 41 genes yielded $p < 10^{-5}$ in one of the two analyses.

We also analyzed a set of 13 previously identified nsCL/P candidate genes with: (1) a significant enrichment of low-frequency variants (four genes),⁶⁰ (2) an autosomal-dominant inheritance pattern in multigenerational families (four genes),⁶¹ or (3) an enrichment of rare coding variants (five genes).⁶² Of these, 12 genes were present in the analysis set. Two of these 12 genes approached test-wide significance: *PRTG* ($p = 8.44 \times 10^{-5}$) and *CTNND1* ($p = 2.17 \times$

10^{-5} ; Table S8). These observations indicate that in at least a subset of genes, both common and rare variations, contribute to nsCL/P.

Genes located in TAD regions of nsCL/P GWAS loci are enriched in developmental pathways

Accumulating evidence suggests that most regulatory interactions occur within TAD modules.^{63,64} Therefore, genes located within TADs represent candidates for the downstream effects of the associated common risk variants. To identify molecular processes of relevance to nsCL/P, for each of the 45 risk loci, GWAS_{TAD} regions were defined, based on the extent of the respective TAD in hESC data.⁴⁰ In total, 407 genes were identified within the respective TADs (GWAS_{TAD} genes, range 1 to 29 genes per locus; Table S9). Enrichment analysis using MAGMA yielded test-wide significant ($p_{\text{adj}} \leq 0.05$) results for 287 GO terms (Table S10). The most significant enrichments were observed for “tissue development” ($p_{\text{adj}} = 8.34 \times 10^{-9}$), “epithelium development” ($p_{\text{adj}} = 8.82 \times 10^{-9}$); and “appendage development” ($p_{\text{adj}} = 7.92 \times 10^{-8}$; Figure S10). Together with additional significant terms, such as “embryo development,” “tube development,” and “ear development,” these observations suggest the existence of common pathways for nsCL/P and other processes of organogenesis during embryonic development.

We then prioritized genes expressed in NCCs by adding available RNA sequencing (RNA-seq) data from hNCCs.⁶⁵ In total, 240 of the 407 GWAS_{TAD} genes were expressed in NCCs, with strong expression being observed for a subset of 12 genes (≥ 200 fragments per kilobase mapped; Table S9). Of these, at least two have been previously implicated in NCC migration processes (*CAPZB*,⁵² *TPM1*⁶⁶). These 240 NCC-expressed genes showed a substantial overlap in significant GO terms compared with the analysis of all 407 GWAS_{TAD} genes (233 out of 287 pathways; Figure 2A; Table S11). Of those 233 pathways, 157 pathways showed stronger enrichment in the subset of NCC-expressed GWAS_{TAD} genes, the strongest of which represent cellular processes (Figure S10; Table S12). Among pathways that were exclusive to GWAS_{TAD} genes expressed in NCCs ($n = 106$), both regulatory processes and metabolic pathways were enriched. In contrast, pathways specific to GWAS_{TAD} genes that were not expressed in NCCs ($n = 54$) included “keratinocyte proliferation” and “epidermis development,” a finding that is consistent with the substantial contribution of the epithelial lineage to nsCL/P.⁵⁶

We next addressed the potential etiological overlap between nsCL/P and other common phenotypes that might contribute to the adverse health outcomes observed in nsCL/P. We retrieved association signals for each of the 45 lead SNPs in MAiC from large-scale genetic studies, using the GWAS ATLAS.⁴⁷ At the time of analysis (November 22, 2019), this resource comprised 4,756 GWASs on 3,302 unique traits. While all of the 45 variants were available in the atlas, only 19 showed at least one significant SNP-trait association when corrected for the number of GWASs and

Table 1. Novel risk loci for nsCL/P identified in MAiC

| Locus | Lead variant | Position ^a | Allele 1/allele 2 ^b | p value | RR ^c | 95% CI |
|------------------------|--------------|-----------------------|--------------------------------|-----------------------|-----------------|-----------|
| 1p36.13 | rs34746930 | 19,781,724 | <u>C</u> /G | 4.19×10^{-8} | 1.30 | 1.18–1.43 |
| 5p12 _{FGF10} | rs60107710 | 44,577,755 | <u>A</u> /G | 3.50×10^{-8} | 1.39 | 1.24–1.57 |
| 5q13 _{PIK3R1} | rs6449957 | 67,483,732 | <u>T</u> /C | 6.59×10^{-9} | 1.21 | 1.13–1.29 |
| 7p21.1 | rs62453366 | 20,747,107 | G/ <u>T</u> | 7.83×10^{-9} | 0.77 | 0.70–0.84 |
| 20q13.12 | rs3091552 | 45,440,006 | <u>C</u> /G | 1.31×10^{-9} | 1.38 | 1.22–1.47 |

nsCL/P, non-syndromic cleft lip with or without cleft palate; MAiC, meta-analysis in clefting; RR, relative risk; CI, confidence interval. Gene names in subscript distinguish novel associated regions from independent risk loci at the same chromosomal band.

^aPosition according to hg19.

^bRisk allele is underlined.

^cRR provided for allele 1.

loci ($p < 2.33 \times 10^{-7}$; overall number: $n = 219$; Table S13). These associations reflect 35 collapsed traits across 12 domains, including height, bone mineral density, hair color, and body mass index (Table S14). Eighteen traits showed associations with at least two distinct nsCL/P risk loci. Interestingly, for some traits, the direction of effect differed between individual loci (e.g., height and bone mineral density), while for other traits, the direction of effect was consistent (e.g., hypothyroidism, glomerular filtration rate, and hair color; Figure 2B).

NsCL/P-associated variants are enriched in multiple chromatin states of mid-facial development

Recent analyses in human embryonic CT³⁹ demonstrated both a significant enrichment of lead SNPs from earlier nsCL/P GWAS in active enhancers and the presence of mid-facial specific regulatory elements. To extend this work, we incorporated data from two NCC states in order to generate a unified mid-facial development resource of chromatin modifications (Figure S1). We retrieved data on ChIP-seq from hNCCs³⁷ and cNCCs³⁸ and applied the data analysis pipeline used by previous authors for computational analyses of ChIP-seq data from CT.³⁹ We observed strong inter-sample correlations between chromatin mark and developmental stage (Figures S11 and S12). The integration of 127 non-facial samples from Roadmap³⁴ revealed local clustering of NCCs and CT along a hierarchical axis comprising hESCs, induced pluripotent stem cells (iPSCs), and iPSC-derived cells (Figure S13). Here, the most tissue-specific pattern was observed for H3K27ac (Figure S14). Similar to a previous finding for CT,³⁹ non-facial fetal tissue samples (such as brain, kidney, and lung) clustered distinctly from NCCs (Figure S14), thus emphasizing the limited utility of many public resources for the interpretation of genetic findings in facial disorders.

Next, we generated robust chromatin segments in NCCs using ChromHMM.⁶⁷ Together with segmentation data from CT and Roadmap, chromatin segments were condensed to eight categories in order to increase the robustness of the subsequent analyses (Figure S15; Table S15). We then analyzed the positional overlap of all variants with $p_{\text{MAiC}} < 0.001$ in the eight chromatin states across NCCs and CT (SNP_{0.001_nsCL/P} $n = 22,999$), and

compared this to a matched set of non-associated SNPs (SNP_{control_nsCL/P} $p > 0.1$). The results showed that 23% of the nsCL/P variants (SNP_{0.001_nsCL/P}) mapped to active chromatin states, while 14% mapped to either bivalent or repressed chromatin states (Figure 3A). This enrichment was significantly higher compared to the control SNPs, where 16% and 11% of variants mapped to active, or to bivalent/repressed, chromatin states, respectively ($p < 10^{-16}$, Fisher's exact test).

To delineate associations of specific chromatin states along the time series, enrichment was tested using GRE-GOR.⁵¹ For each of the two SNP sets, every hNCC/cNCC/CT sample was tested, together with 11 randomly selected Roadmap samples (both fetal and adult). A significant enrichment for SNP_{0.01_nsCL/P} was observed in most of the samples/chromatin states (Figure 3B; Table S16), as compared to SNP_{control_nsCL/P} (Figure S16; Table S17). While the fold enrichment (FE) was similar for NCCs and CT in six of the eight chromatin states (such as those related to active transcription; Figures 4A–4D; Figure S17), considerable differences in enrichment between NCC and CT samples were observed in chromatin states “active enhancers” and “poised enhancers/bivalent TSS.” In both states, NCCs displayed a stronger enrichment than CT samples. For enhancers, the mean FE (FE_{Mean}) in NCCs was 1.64 ($p_{\text{Mean}} = 4.36 \times 10^{-86}$, average of p_{GREGOR}), compared with FE_{Mean} = 1.43 in CT ($p_{\text{Mean}} = 8.09 \times 10^{-22}$). For “poised enhancers/bivalent TSS,” the corresponding values were FE_{Mean} = 1.65, $p_{\text{Mean}} = 3.39 \times 10^{-20}$ in NCCs, compared with FE_{Mean} = 1.39, $p_{\text{Mean}} = 4.74 \times 10^{-4}$ in CT. These results may have been driven in part by the heterogeneous composition of the CT samples. However, the specific enrichment pattern observed in two out of eight chromatin states suggests a distinct biological underpinning. Overall, these data confirmed previous findings of an over-representation of nsCL/P lead variants in enhancer marks^{21,39} and extended this enrichment toward additional common variants and annotations.

A subset of nsCL/P-associated SNPs show distinct regulatory effects

To extend the investigation of the contribution of regions with differing regulatory profiles in NCCs and CT, we

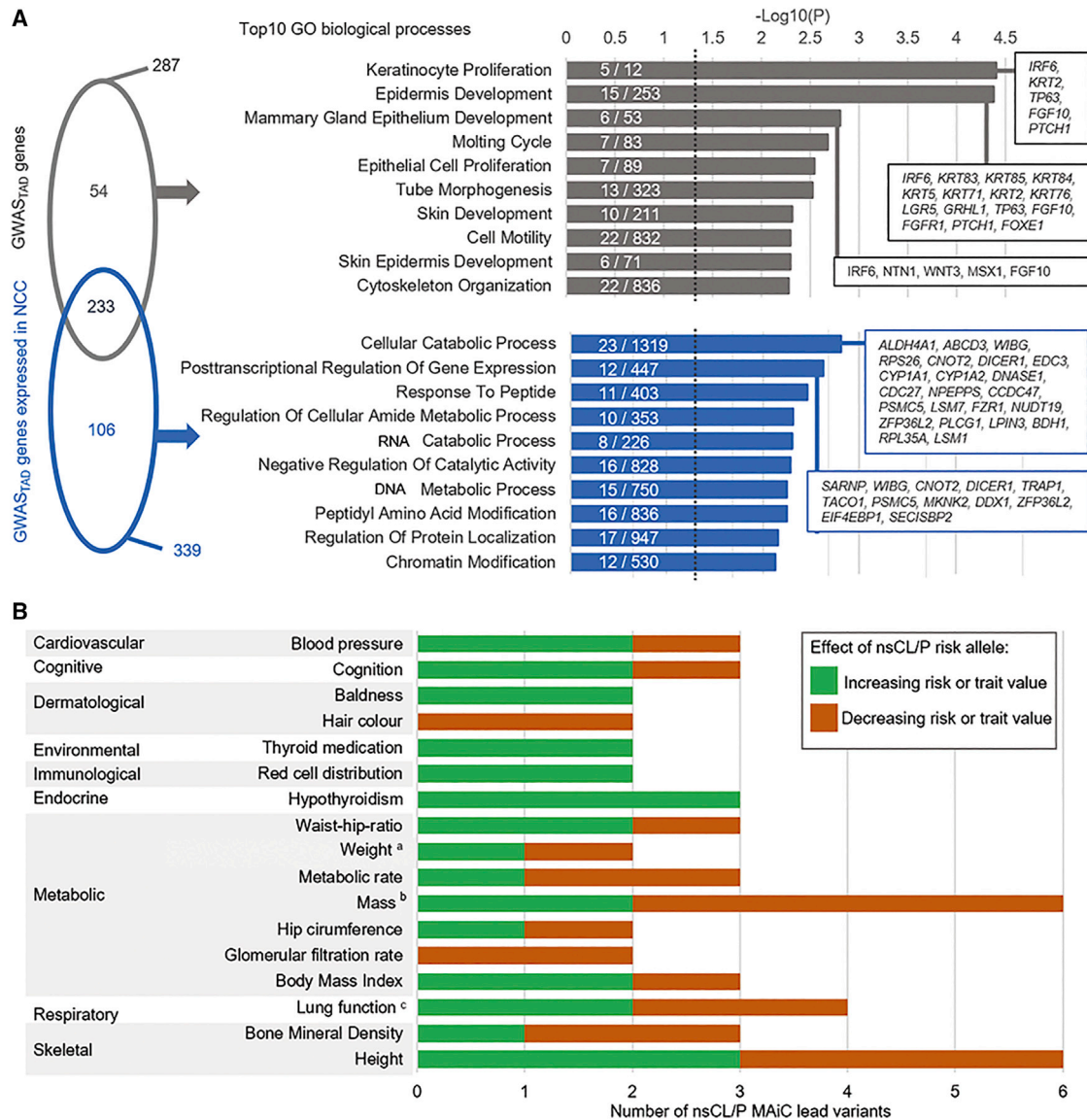


Figure 2. Systematic assessment of 45 risk loci for nsCL/P

(A) Enrichment analyses of biological processes. Enrichment of genes located at risk loci identified by genome-wide association studies (GWAS_{TAD} genes, $n = 407$, gray) and the subset of genes expressed in neural crest cells ($n = 240$, blue) were calculated using MAGMA. Left panel: While most of the associated pathways overlapped both datasets, a subset of terms was distinctly enriched in one of the groups. Right panel: Bars represent the top 10 of each specific enrichment ($p_{adj} \leq 0.05$). Numbers reflect nsCL/P risk genes/total number of genes in the respective gene ontology (GO) term. For the most strongly associated pathways, gene names are provided in the respective box. (B) Pleiotropic effects of lead variants. For the lead variant of each of the 45 nsCL/P risk loci, associations with common traits were retrieved from the GWAS ATLAS. Associations with at least two risk loci were observed for 17 traits from 12 domains (y axis). Bar colors represent direction of effects. ^aIncluding birth weight. ^bIncluding multiple mass-related measurements. ^cLung function as measured by Forced expiratory volume (FEV)₁ or FEV₁/Forced vital capacity (FVC) ratio.

created genome-wide maps of active chromatin sites for both NCCs and CT. A total of 9,897 regions (encompassing 26.67 Mb) with active chromatin states in NCCs (TSS, enhancer or transcribed sites) were inactive in CT (quiescent, repressed, or bivalent; termed NCC-specific active sites). Similarly, 6,189 regions (29.37 Mb) were active in CT but inactive in NCCs (CT-specific active sites). The integration of MAiC association data revealed 62,084 genetic variants that map in NCC-specific active sites. Of these, 4,022 had $p_{MAiC} \leq 0.05$. Similarly, 72,556 variants (4,834 of which had $p_{MAiC} \leq 0.05$) mapped to CT-specific active

sites. In each of the groups of NCC-specific and CT-specific active sites, the p value distribution differed significantly from that expected, with a significant enrichment of association signals being observed at the lower tail of the distribution (Figure 5A).

Filtering for the subset of SNPs with $p_{MAiC} \leq 5 \times 10^{-5}$ identified 112 SNPs that mapped to either NCC-specific (51 variants), or CT-specific active regions (61 variants; Table S18). These were distributed over 39 TADs, which encompassed both known nsCL/P risk loci ($n = 19$; e.g., chromosomes 1p22 [Figure S18] and 2p24.2 [Figure S19]) and

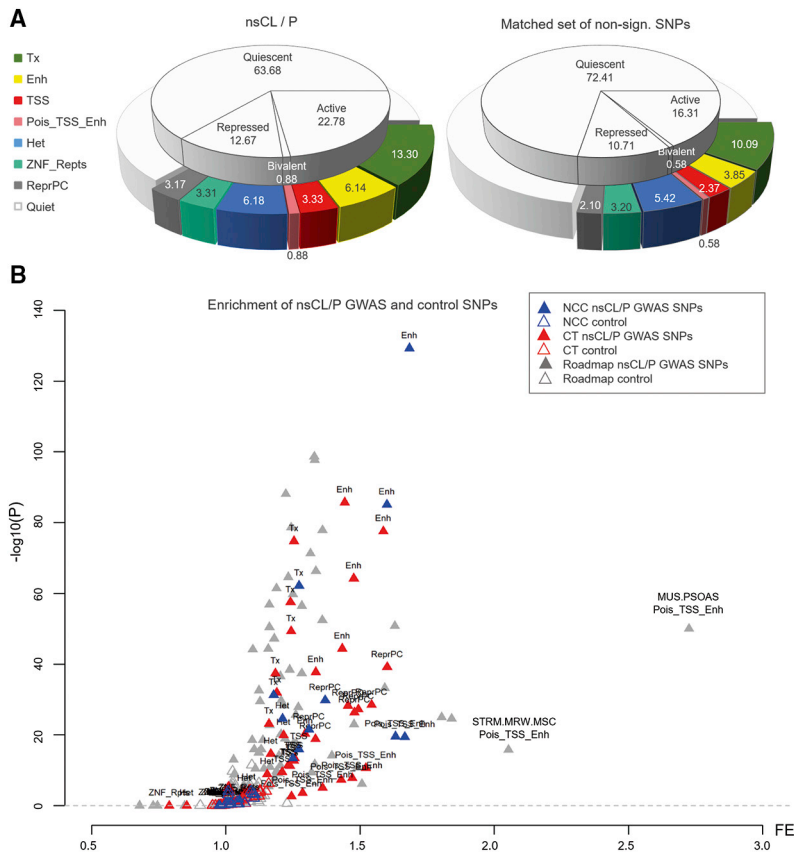


Figure 3. Association of MAiC across epigenetic annotations

For all enrichment analyses, two sets of single-nucleotide polymorphisms (SNPs) were designed: (1) set of MAiC risk variants, at $p_{\text{MAiC}} \leq 0.001$ ($n = 22,999$), and (2) a size-matched control set, comprising non-associated SNPs ($p_{\text{MAiC}} > 0.1$) with similar allele-frequency distribution.

(A) Overall enrichment analysis. For each group, the fraction of SNPs represented in different chromatin annotations of mid-facial development was assessed, without discriminating between NCCs and craniofacial tissue (CT).

(B) Overview of enrichment in NCCs and CT. Enrichment of nsCL/P risk variants in eight chromatin states for each sample (hNCCs, cNCCs, and CT, plus a set of 11 Roadmap samples). p values were calculated using GREGOR.⁵¹ Abbreviations: TSS, transcription starting site; Enh, enhancer; ReprPC, repressed PolyComb; Tx, transcribed sites; Het, Heterochromatin; TxFlnk, transcribed sites at gene 5' and 3'; Pois_TSS_Enh, poised enhancers and bivalent TSS; ZNF_Rpts, Zinc finger genes and repeats; FE, fold enrichment. Abbreviations of tissues as provided by Roadmap.³⁴

regions with suggestive evidence for association ($n = 20$; e.g., chromosome 4p13 [Figure S20]). Interestingly, at six loci (e.g., chromosomes 1q32.1 [Figure S21] and 15q24.1 [Figure S22]), at least two associated variants in LD were located in different specific elements (Table S19). This represents a significantly higher enrichment than expected and suggests that individual variants of risk haplotypes might affect the regulatory architecture at different stages of craniofacial development (Figure 5B).

Finally, we assessed how novel hypotheses on nsCL/P pathogenesis can be generated from the systematic integration of data concerning: (1) statistical associations (MAiC), (2) chromatin modifications over time (mid-facial time-series), and (3) pChI-C *cis*-interactions.⁴¹ Examples from two loci are described here. First, at 5q13_{PIK3R1}, the lead variant (rs6449957, $p_{\text{MAiC}} = 6.59 \times 10^{-10}$) is located within an active region upstream of *PIK3R1*. This region shows evidence of being transcribed but lacks any RefSeq annotation, which might point toward a transcribed enhancer or an as-yet-undetected transcript. PChI-C data indicate *cis* interactions with *PIK3R1* and *MAST4*, both of which are expressed in hNCCs. In addition, another variant in strong LD (rs921792, $p_{\text{MAiC}} = 1.17 \times 10^{-5}$) maps to a putative enhancer that is detected in both NCCs and CT (Figure 5C). As a second example, at 13q32.2 (lead variant rs2763950, $p_{\text{MAiC}} = 3.03 \times 10^{-6}$, intronic in *CLYBL*), interactions were observed between the region around the lead variant and the genes *ZIC2*, *ZIC5*, and *GGACT*. While

some variants (including rs2763934 with $p_{\text{MAiC}} = 6.53 \times 10^{-7}$) map to a craniofacial active element near the *CLYBL* gene promoter, additional variants (including rs4525350 with $p_{\text{MAiC}} = 6.39 \times 10^{-6}$) map to several more distantly located NCC-specific enhancers.

Based on pChI-C data, our data indicate that in NCCs, risk variants might affect *ZIC2* and *ZIC5* expression. This hypothesis is further supported by the finding of active transcription sites in NCCs and a bivalent state in embryonic and adult tissues. A plausible hypothesis is that, at later time points of development, additional variants mapping to other enhancer elements act on *GGACT*, as suggested by the presence of transcribed sites in CT. Notably, the transcript region of *CLYBL* itself has limited evidence for active transcription across all analyzed stages of mid-facial development, despite the presence of some active marks in the promoter region (Figure 5D).

At other loci, our data provide evidence for the presence of tissue-specific gene isoforms (e.g., 4p13-locus; Figure S20), or a second, novel candidate gene at previously reported loci. For example, at chromosome 1p22, our data suggest that the previously identified gene *ARHGAP29*³⁶ is a target gene with CT-specific expression and highlight *ABCD3* as novel candidate gene (Figure S18). The data also suggest complex promoter-promoter interactions involving all genes at this locus (*ARHGAP29*, *ABCD3*, and *ABCA4*). Interestingly, the MAiC top-associated variant at 1p22 (rs35298667, $p_{\text{MAiC}} = 6.86 \times 10^{-16}$) has putative enhancer function and maps to the “E2” element, whose functional role in nsCL/P was confirmed in previous research.³² At another locus (1q32.1), we found that *SERTAD4* is a CT-specific target gene, while the established causal gene *IRF6* was marked as bivalent, which

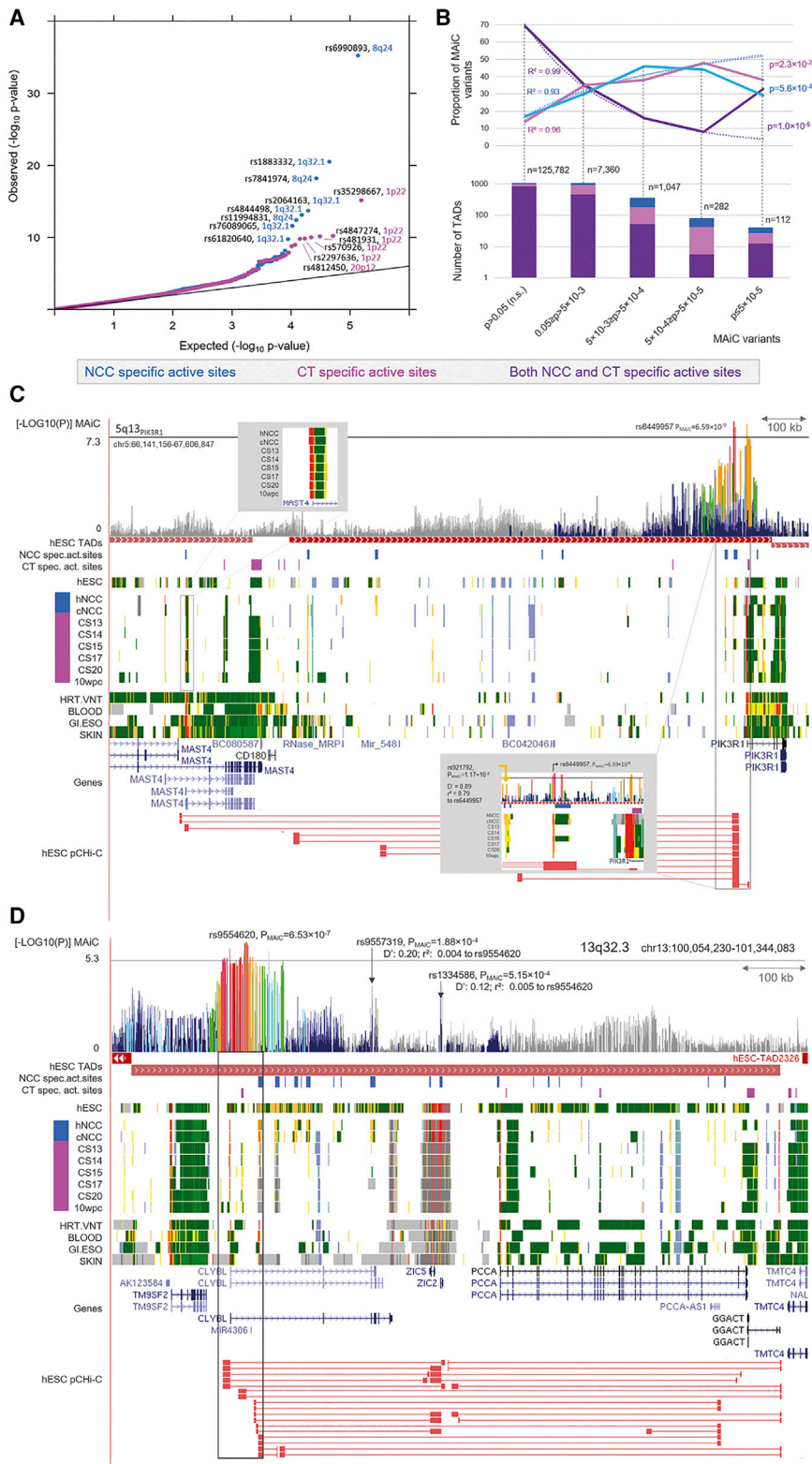


Figure 5. Interpretation of MAiC association results

(A) Quantile-quantile plot of specific active sites. P_{MAiC} values (as $-\log_{10}$) of SNPs located in NCC-specific ($n = 62,084$; blue) or CT-specific ($n = 72,556$; pink) active sites are plotted against expected p values. In both datasets, a significant enrichment of associated risk variants was observed.

(B) Distribution of risk variants in specific active sites. Variants located within NCC- and CT-specific regions were retrieved at different P_{MAiC} cutoffs and aggregated per topologically associated domain (TAD, numbers in lower panel). TADs were classified according to whether the variants map uniquely to NCC-active elements (blue), CT-specific elements (pink), or both (purple). The distribution largely followed the expected logarithmic distribution. However, for a substantial number of loci, different associated SNPs (at $p < 5 \times 10^{-5}$) mapped to both NCC- and CT-specific sites within one TAD.

(C and D) Regulatory architecture at selected loci. Based on the extent of the TAD around the respective lead variant and variants in LD ≥ 0.6 (shown in gray framed box), different layers of data were aggregated and are represented for risk loci 5q13_{PIK3R1} (C) and 13q32.3 (D). Tracks include (top-down): MAiC p values with color code based on LD to respective top variants; extent of NCC-specific (blue) and CT-specific (pink) sites; chromatin segmentation data from hNCCs, cNCCs, CT (color code as in Figure 3), and selected samples from Roadmap; RefSeq gene positions; and promoter capture (pC) Hi-C *cis*-interactions collected in hESCs.

ARHGAP29^{76,77} and *IRF6*²⁵), or experimental evidence (e.g., *PAX7*⁷⁸). While we here focused on an *in silico* approach, we hope that the results will empower further experimental investigations of specific risk variants that were highlighted among the set of associated variants. Using the joint pipeline, we will continue to update our resource as chromatin marks become available from additional human tissues and/or cell systems of relevance to mid-facial development. In addition, the map will be refined through the use of single-cell technol-

ogies in order to resolve the issue of tissue heterogeneity encountered in the present study. Finally, the integration of other layers of genetic information, such as rare variants identified by whole-exome or -genome sequencing in cleft cohorts, will further increase our understanding of the etiology of craniofacial development and disease.^{61,79}

architecture, and several genes at single loci might be of relevance across the different time points of craniofacial development. Notably, several of the genes prioritized by our systematic approach have obtained independent support by other studies, for instance clefting syndromes (e.g., *TP63*, EEC syndrome⁷⁵), resequencing studies (e.g.,

Data and code availability

Original data for genetic and functional analyses in the paper is available as follows: dbGaP (dbGaP: phs000094 and phs000774), GEO (GEO: GSE28874, GSE70751, and GSE97752), and Zenodo (DOI 10.5281/zenodo.3724148). The NCC- and CT-specific active sites generated during this study are available at Zenodo (DOI 10.5281/zenodo.3911187).

Supplemental information

Supplemental information can be found online at <https://doi.org/10.1016/j.xhgg.2021.100038>.

Acknowledgments

We thank Markus M. Nöthen and Andreas Bunes for helpful discussions on the manuscript and Carlo Maj for data management. This work was supported by the German Research Foundation (DFG; LU 1944/3-1, to K.U.L.).

Declaration of interests

The authors declare no competing interests.

Received: January 19, 2021

Accepted: May 27, 2021

Web resources

ANNOVAR, <https://wglab.org/software/9-annovar>
Bowtie2, <http://bowtie-bio.sourceforge.net/bowtie2/index.shtml>
ChromHMM, <http://compbio.mit.edu/ChromHMM/>
ChromImpute, <http://www.biolchem.ucla.edu/labs/ernst/ChromImpute/>
core 15-state chromatin model, <https://egg2.wustl.edu/roadmap/data/byFileType/chromhmmSegmentations/ChmmModels/>
FastQC, <https://www.bioinformatics.babraham.ac.uk/projects/fastqc>
FUMA, <https://fuma.ctglab.nl/>
GREGOR, <http://csg.sph.umich.edu/GREGOR/>
GTEx, <https://www.gtexportal.org/home/>
GWAS Atlas, <https://atlas.ctglab.nl/>
Hi-C data from Bing Ren Lab, <http://chromosome.sdsc.edu/mouse/hi-c/download.html>
IMPUTE2, http://mathgen.stats.ox.ac.uk/impute/impute_v2.html
KING: Kinship-based Inference for GWAS, <https://www.kingrelatedness.com/>
LDlink, <https://ldlink.nci.nih.gov/?tab=home>
LDSR, <http://ldsc.broadinstitute.org/ldhub/>
MACS2, <https://github.com/macs3-project/MACS>
MAGMA, <https://ctg.cncr.nl/software/magma>
METAL, <http://csg.sph.umich.edu/abecasis/metal/>
MSigDB, <https://www.gsea-msigdb.org/gsea/msigdb/index.jsp>
PhantomPeakQualTools, <https://github.com/kundajelab/phantompeakqualtools>
Roadmap, <https://egg2.wustl.edu/roadmap/data/byFileType/signal/consolidated/macs2signal/pval/>
UCSC, <http://genome.ucsc.edu/>

References

1. Claussnitzer, M., Dankel, S.N., Kim, K.-H., Quon, G., Meuleman, W., Haugen, C., Glunk, V., Sousa, I.S., Beaudry, J.L., Puvion-Rodan, V., et al. (2015). FTO Obesity Variant Circuitry and Adipocyte Browning in Humans. *N. Engl. J. Med.* 373, 895–907.
2. Xue, A., Wu, Y., Zhu, Z., Zhang, F., Kemper, K.E., Zheng, Z., Yengo, L., Lloyd-Jones, L.R., Sidorenko, J., Wu, Y., et al.; eQTL-Gen Consortium (2018). Genome-wide association analyses identify 143 risk variants and putative regulatory mechanisms for type 2 diabetes. *Nat. Commun.* 9, 2941.
3. Markunas, C.A., Johnson, E.O., and Hancock, D.B. (2017). Comprehensive evaluation of disease- and trait-specific enrichment for eight functional elements among GWAS-identified variants. *Hum. Genet.* 136, 911–919.
4. Visscher, P.M., Wray, N.R., Zhang, Q., Sklar, P., McCarthy, M.I., Brown, M.A., and Yang, J. (2017). 10 Years of GWAS Discovery: Biology, Function, and Translation. *Am. J. Hum. Genet.* 101, 5–22.
5. Roman, T.S., and Mohlke, K.L. (2018). Functional genomics and assays of regulatory activity detect mechanisms at loci for lipid traits and coronary artery disease. *Curr. Opin. Genet. Dev.* 50, 52–59.
6. Lu, Q., Powles, R.L., Abdallah, S., Ou, D., Wang, Q., Hu, Y., Lu, Y., Liu, W., Li, B., Mukherjee, S., et al. (2017). Systematic tissue-specific functional annotation of the human genome highlights immune-related DNA elements for late-onset Alzheimer's disease. *PLoS Genet.* 13, e1006933.
7. Claussnitzer, M., Cho, J.H., Collins, R., Cox, N.J., Dermitzakis, E.T., Hurles, M.E., Kathiresan, S., Kenny, E.E., Lindgren, C.M., MacArthur, D.G., et al. (2020). A brief history of human disease genetics. *Nature* 577, 179–189.
8. Jugessur, A., Farlie, P.G., and Kilpatrick, N. (2009). The genetics of isolated orofacial clefts: From genotypes to subphenotypes. *Oral Dis* 15, 437–453.
9. Mangold, E., Ludwig, K.U., and Nöthen, M.M. (2011). Breakthroughs in the genetics of orofacial clefting. *Trends Mol. Med.* 17, 725–733.
10. Mossey, P.A., and Modell, B. (2012). Epidemiology of oral clefts 2012: An international perspective. *Front. Oral Biol* 16, 1–18.
11. Grosen, D., Bille, C., Pedersen, J.K., Skytthe, A., Murray, J.C., and Christensen, K. (2010). Recurrence risk for offspring of twins discordant for oral cleft: A population-based cohort study of the Danish 1936-2004 cleft twin cohort. *Am. J. Med. Genet. A* 152A, 2468–2474.
12. Christensen, K., Juel, K., Herskind, A.M., and Murray, J.C. (2004). Long term follow up study of survival associated with cleft lip and palate at birth. *BMJ* 328, 1405.
13. Yu, Y., Zuo, X., He, M., Gao, J., Fu, Y., Qin, C., Meng, L., Wang, W., Song, Y., Cheng, Y., et al. (2017). Genome-wide analyses of non-syndromic cleft lip with palate identify 14 novel loci and genetic heterogeneity. *Nat. Commun.* 8, 14364.
14. van Rooij, I.A., Ludwig, K.U., Welzenbach, J., Ishorst, N., Thonissen, M., Galesloot, T.E., Ongkosuwito, E., Bergé, S.J., Aldhore, K., Rojas-Martinez, A., et al. (2019). Non-syndromic cleft lip with or without cleft palate: Genome-wide association study in Europeans identifies a suggestive risk locus at 16p12.1 and supports SH3PXD2A as a clefting susceptibility gene. *Genes (Basel)* 10, 1023.
15. Moreno, L.M., Mansilla, M.A., Bullard, S.A., Cooper, M.E., Busch, T.D., Machida, J., Johnson, M.K., Brauer, D., Krahn, K., Daack-Hirsch, S., et al. (2009). FOXE1 association with both isolated cleft lip with or without cleft palate, and isolated cleft palate. *Hum. Mol. Genet.* 18, 4879–4896.

16. Mostowska, A., Gaczowska, A., Żukowski, K., Ludwig, K.U., Hozyasz, K.K., Wójcicki, P., Mangold, E., Böhmer, A.C., Heilmann-Heimbach, S., Knapp, M., et al. (2018). Common variants in DLG1 locus are associated with non-syndromic cleft lip with or without cleft palate. *Clin. Genet.* *93*, 784–793.
17. Leslie, E.J., Carlson, J.C., Shaffer, J.R., Feingold, E., Wehby, G., Laurie, C.A., Jain, D., Laurie, C.C., Doheny, K.F., McHenry, T., et al. (2016). A multi-ethnic genome-wide association study identifies novel loci for non-syndromic cleft lip with or without cleft palate on 2p24.2, 17q23 and 19q13. *Hum. Mol. Genet.* *25*, 2862–2872.
18. Mangold, E., Ludwig, K.U., Birnbaum, S., Baluardo, C., Ferrian, M., Herms, S., Reutter, H., de Assis, N.A., Chawa, T.A., Mattheisen, M., et al. (2010). Genome-wide association study identifies two susceptibility loci for nonsyndromic cleft lip with or without cleft palate. *Nat. Genet.* *42*, 24–26.
19. Ludwig, K.U., Mangold, E., Herms, S., Nowak, S., Reutter, H., Paul, A., Becker, J., Herberz, R., AlChawa, T., Nasser, E., et al. (2012). Genome-wide meta-analyses of nonsyndromic cleft lip with or without cleft palate identify six new risk loci. *Nat. Genet.* *44*, 968–971.
20. Beaty, T.H., Murray, J.C., Marazita, M.L., Munger, R.G., Ruczinski, I., Hetmanski, J.B., Liang, K.Y., Wu, T., Murray, T., Fallin, M.D., et al. (2010). A genome-wide association study of cleft lip with and without cleft palate identifies risk variants near MAFB and ABCA4. *Nat. Genet.* *42*, 525–529.
21. Ludwig, K.U., Böhmer, A.C., Bowes, J., Nikolić, M., Ishorst, N., Wyatt, N., Hammond, N.L., Gözl, L., Thieme, F., Barth, S., et al. (2017). Imputation of orofacial clefting data identifies novel risk loci and sheds light on the genetic background of cleft lip ± cleft palate and cleft palate only. *Hum. Mol. Genet.* *26*, 829–842.
22. Sun, Y., Huang, Y., Yin, A., Pan, Y., Wang, Y., Wang, C., Du, Y., Wang, M., Lan, F., Hu, Z., et al. (2015). Genome-wide association study identifies a new susceptibility locus for cleft lip with or without a cleft palate. *Nat. Commun.* *6*, 6414.
23. Ludwig, K.U., Ahmed, S.T., Böhmer, A.C., Sangani, N.B., Varghese, S., Klamt, J., Schuenke, H., Gültepe, P., Hofmann, A., Rubini, M., et al. (2016). Meta-analysis Reveals Genome-Wide Significance at 15q13 for Nonsyndromic Clefting of Both the Lip and the Palate, and Functional Analyses Implicate GREM1 As a Plausible Causative Gene. *PLoS Genet.* *12*, e1005914.
24. Beaty, T.H., Taub, M.A., Scott, A.F., Murray, J.C., Marazita, M.L., Schwender, H., Parker, M.M., Hetmanski, J.B., Balakrishnan, P., Mansilla, M.A., et al. (2013). Confirming genes influencing risk to cleft lip with/without cleft palate in a case-parent trio study. *Hum. Genet.* *132*, 771–781.
25. Zuccherro, T.M., Cooper, M.E., Maher, B.S., Daack-Hirsch, S., Nepomuceno, B., Ribeiro, L., Caprau, D., Christensen, K., Suzuki, Y., Machida, J., et al. (2004). Interferon Regulatory Factor 6 (IRF6) Gene Variants and the Risk of Isolated Cleft Lip or Palate. *N. Engl. J. Med.* *351*, 769–780.
26. Leslie, E.J., Carlson, J.C., Shaffer, J.R., Butali, A., Buxó, C.J., Castilla, E.E., Christensen, K., Deleyiannis, F.W.B., Leigh Field, L., Hecht, J.T., et al. (2017). Genome-wide meta-analyses of nonsyndromic orofacial clefts identify novel associations between FOXE1 and all orofacial clefts, and TP63 and cleft lip with or without cleft palate. *Hum. Genet.* *136*, 275–286.
27. Birnbaum, S., Ludwig, K.U., Reutter, H., Herms, S., Steffens, M., Rubini, M., Baluardo, C., Ferrian, M., Almeida de Assis, N., Alblas, M.A., et al. (2009). Key susceptibility locus for non-syndromic cleft lip with or without cleft palate on chromosome 8q24. *Nat. Genet.* *41*, 473–477.
28. Rahimov, F., Marazita, M.L., Visel, A., Cooper, M.E., Hitchler, M.J., Rubini, M., Domann, F.E., Govil, M., Christensen, K., Bille, C., et al. (2008). Disruption of an AP-2 α binding site in an IRF6 enhancer is associated with cleft lip. *Nat. Genet.* *40*, 1341–1347.
29. Thieme, F., and Ludwig, K.U. (2017). The Role of Noncoding Genetic Variation in Isolated Orofacial Clefts. *J. Dent. Res.* *96*, 1238–1247.
30. Attanasio, C., Nord, A.S., Zhu, Y., Blow, M.J., Li, Z., Liberton, D.K., Morrison, H., Plajzer-Frick, I., Holt, A., Hosseini, R., et al. (2013). Fine tuning of craniofacial morphology by distant-acting enhancers. *Science* *342*, 1241006.
31. Uslu, V.V., Petretich, M., Ruf, S., Langenfeld, K., Fonseca, N.A., Marioni, J.C., and Spitz, F. (2014). Long-range enhancers regulating Myc expression are required for normal facial morphogenesis. *Nat. Genet.* *46*, 753–758.
32. Liu, H., Leslie, E.J., Carlson, J.C., Beaty, T.H., Marazita, M.L., Lidral, A.C., and Cornell, R.A. (2017). Identification of common non-coding variants at 1p22 that are functional for non-syndromic orofacial clefting. *Nat. Commun.* *8*, 14759.
33. Dunham, I., Kundaje, A., Aldred, S.F., Collins, P.J., Davis, C.A., Doyle, F., Epstein, C.B., Frietze, S., Harrow, J., Kaul, R., et al.; ENCODE Project Consortium (2012). An integrated encyclopedia of DNA elements in the human genome. *Nature* *489*, 57–74.
34. Kundaje, A., Meuleman, W., Ernst, J., Bilenky, M., Yen, A., Heravi-Moussavi, A., Kheradpour, P., Zhang, Z., Wang, J., Ziller, M.J., et al.; Roadmap Epigenomics Consortium (2015). Integrative analysis of 111 reference human epigenomes. *Nature* *518*, 317–330.
35. Aguet, F., Brown, A.A., Castel, S.E., Davis, J.R., He, Y., Jo, B., Mohammadi, P., Park, Y.S., Parsana, P., Segrè, A.V., et al. (2017). Genetic effects on gene expression across human tissues. *Nature* *550*, 204–213.
36. Leslie, E.J., Mansilla, M.A., Biggs, L.C., Schuette, K., Bullard, S., Cooper, M., Dunnwald, M., Lidral, A.C., Marazita, M.L., Beaty, T.H., et al. (2012). Expression and mutation analyses implicate ARHGAP29 as the etiologic gene for the cleft lip with or without cleft palate locus identified by genome-wide association on chromosome 1p22. *Birth Defects Res. A Clin. Mol. Teratol.* *94*, 934–942.
37. Rada-Iglesias, A., Bajpai, R., Prescott, S., Brugmann, S.A., Swigut, T., and Wysocka, J. (2012). Epigenomic annotation of enhancers predicts transcriptional regulators of human neural crest. *Cell Stem Cell* *11*, 633–648.
38. Prescott, S.L., Srinivasan, R., Marchetto, M.C., Grishina, I., Narvaiza, I., Selleri, L., Gage, F.H., Swigut, T., and Wysocka, J. (2015). Enhancer divergence and cis-regulatory evolution in the human and chimp neural crest. *Cell* *163*, 68–83.
39. Wilderman, A., VanOudenhove, J., Kron, J., Noonan, J.P., and Cotney, J. (2018). High-Resolution Epigenomic Atlas of Human Embryonic Craniofacial Development. *Cell Rep* *23*, 1581–1597.
40. Dixon, J.R., Selvaraj, S., Yue, F., Kim, A., Li, Y., Shen, Y., Hu, M., Liu, J.S., and Ren, B. (2012). Topological domains in mammalian genomes identified by analysis of chromatin interactions. *Nature* *485*, 376–380.
41. Freire-Pritchett, P., Schoenfelder, S., Várnai, C., Wingett, S.W., Cairns, J., Collier, A.J., García-Vílchez, R., Furlan-Magaril, M., Osborne, C.S., Fraser, P., et al. (2017). Global reorganisation

- of *cis*-regulatory units upon lineage commitment of human embryonic stem cells. *eLife* 6, e21926.
42. Marchini, J., Howie, B., Myers, S., McVean, G., and Donnelly, P. (2007). A new multipoint method for genome-wide association studies by imputation of genotypes. *Nat. Genet.* 39, 906–913.
 43. Spielman, R.S., McGinnis, R.E., and Ewens, W.J. (1993). Transmission test for linkage disequilibrium: the insulin gene region and insulin-dependent diabetes mellitus (IDDM). *Am. J. Hum. Genet.* 52, 506–516.
 44. Willer, C.J., Li, Y., and Abecasis, G.R. (2010). METAL: fast and efficient meta-analysis of genomewide association scans. *Bioinformatics* 26, 2190–2191.
 45. Bulik-Sullivan, B.K., Loh, P.R., Finucane, H.K., Ripke, S., Yang, J., Patterson, N., Daly, M.J., Price, A.L., Neale, B.M., Corvin, A., et al.; Schizophrenia Working Group of the Psychiatric Genomics Consortium (2015). LD Score regression distinguishes confounding from polygenicity in genome-wide association studies. *Nat. Genet.* 47, 291–295.
 46. de Leeuw, C.A., Mooij, J.M., Heskes, T., and Posthuma, D. (2015). MAGMA: Generalized Gene-Set Analysis of GWAS Data. *PLoS Comput. Biol.* 11, e1004219.
 47. Watanabe, K., Stringer, S., Frei, O., Umičević Mirkov, M., de Leeuw, C., Polderman, T.J.C., van der Sluis, S., Andreassen, O.A., Neale, B.M., and Posthuma, D. (2019). A global overview of pleiotropy and genetic architecture in complex traits. *Nat. Genet.* 51, 1339–1348.
 48. Ernst, J., and Kellis, M. (2015). Large-scale imputation of epigenomic datasets for systematic annotation of diverse human tissues. *Nat. Biotechnol.* 33, 364–376.
 49. Ernst, J., and Kellis, M. (2017). Chromatin-state discovery and genome annotation with ChromHMM. *Nat. Protoc.* 12, 2478–2492.
 50. Lausch, M., Bartusel, M., Alirzayeva, H., Karaolidou, A., Rehim, R., Crispatzu, G., Nikolic, M., Bleckwehl, T., Kolovos, P., van Ijcken, W.F.J., et al. (2018). Disruption of the TFAP2A Regulatory Domain Causes Banchio-Oculo-Facial Syndrome (BOFS) and Illuminates Pathomechanisms for Other Human Neurocristopathies. *Cell Stem Cell* 24, 736–752, e12.
 51. Schmidt, E.M., Zhang, J., Zhou, W., Chen, J., Mohlke, K.L., Chen, Y.E., and Willer, C.J. (2015). GREGOR: evaluating global enrichment of trait-associated variants in epigenomic features using a systematic, data-driven approach. *Bioinformatics* 31, 2601–2606.
 52. Mukherjee, K., Ishii, K., Pillalammarri, V., Kammin, T., Atkin, J.F., Hickey, S.E., Xi, Q.J., Zepeda, C.J., Gusella, J.F., Talkowski, M.E., et al. (2016). Actin capping protein CAPZB regulates cell morphology, differentiation, and neural crest migration in craniofacial morphogenesis. *Hum. Mol. Genet.* 25, 1255–1270.
 53. McLennan, R., Bailey, C.M., Schumacher, L.J., Teddy, J.M., Morrison, J.A., Kasemeier-Kulesa, J.C., Wolfe, L.A., Gogol, M.M., Baker, R.E., Maini, P.K., et al. (2017). DAN (NBL1) promotes collective neural crest migration by restraining uncontrolled invasion. *J. Cell Biol.* 16, 3339–3354.
 54. Matt, N., Dupé, V., Garnier, J.M., Dennefeld, C., Chambon, P., Mark, M., and Ghyselinck, N.B. (2005). Retinoic acid-dependent eye morphogenesis is orchestrated by neural crest cells. *Development* 132, 4789–4800.
 55. Kousa, Y.A., Fuller, E., and Schutte, B.C. (2018). IRF6 and AP2A Interaction Regulates Epidermal Development. *J. Invest. Dermatol.* 138, 2578–2588.
 56. Lin-Shiao, E., Lan, Y., Welzenbach, J., Alexander, K.A., Zhang, Z., Knapp, M., Mangold, E., Sammons, M., Ludwig, K.U., and Berger, S.L. (2019). p63 establishes epithelial enhancers at critical craniofacial development genes. *Sci. Adv.* 5, eaaw0946.
 57. Kobayashi, K., Jakt, L.M., and Nishikawa, S.I. (2013). Epigenetic regulation of the neuroblastoma genes, *Arid3b* and *Mycn*. *Oncogene* 32, 2640–2648.
 58. Takebe, A., Era, T., Okada, M., Martin Jakt, L., Kuroda, Y., and Nishikawa, S. (2006). Microarray analysis of PDGFR α + populations in ES cell differentiation culture identifies genes involved in differentiation of mesoderm and mesenchyme including ARID3b that is essential for development of embryonic mesenchymal cells. *Dev. Biol.* 293, 25–37.
 59. Jakobsen, L.P., Borup, R., Vestergaard, J., Larsen, L.A., Lage, K., Maroun, L.L., Kjaer, I., Niemann, C.U., Andersen, M., Knudsen, M.A., et al. (2009). Expression analyses of human cleft palate tissue suggest a role for osteopontin and immune related factors in palatal development. *Exp. Mol. Med.* 41, 77–85.
 60. Leslie, E.J., Carlson, J.C., Shaffer, J.R., Buxó, C.J., Castilla, E.E., Christensen, K., Deleyiannis, F.W.B., Field, L.L., Hecht, J.T., Moreno, L., et al. (2017). Association studies of low-frequency coding variants in nonsyndromic cleft lip with or without cleft palate. *Am. J. Med. Genet. A* 173, 1531–1538.
 61. Cox, L.L., Cox, T.C., Moreno Uribe, L.M., Zhu, Y., Richter, C.T., Nidey, N., Standley, J.M., Deng, M., Blue, E., Chong, J.X., et al. (2018). Mutations in the Epithelial Cadherin-p120-Catenin Complex Cause Mendelian Non-Syndromic Cleft Lip with or without Cleft Palate. *Am. J. Hum. Genet.* 102, 1143–1157.
 62. Marini, N.J., Asrani, K., Yang, W., Rine, J., and Shaw, G.M. (2019). Accumulation of rare coding variants in genes implicated in risk of human cleft lip with or without cleft palate. *Am. J. Med. Genet. A* 179, 1260–1269.
 63. Lupiáñez, D.G., Spielmann, M., and Mundlos, S. (2016). Breaking TADs: How Alterations of Chromatin Domains Result in Disease. *Trends Genet.* 32, 225–237.
 64. Lupiáñez, D.G., Kraft, K., Heinrich, V., Krawitz, P., Brancati, F., Klopocki, E., Horn, D., Kayserili, H., Opitz, J.M., Laxova, R., et al. (2015). Disruptions of topological chromatin domains cause pathogenic rewiring of gene-enhancer interactions. *Cell* 161, 1012–1025.
 65. Lausch, M., Bartusel, M., Rehim, R., Alirzayeva, H., Karaolidou, A., Crispatzu, G., Zentis, P., Nikolic, M., Bleckwehl, T., Kolovos, P., et al. (2019). Modeling the Pathological Long-Range Regulatory Effects of Human Structural Variation with Patient-Specific hiPSCs. *Cell Stem Cell* 24, 736–752.e12.
 66. Vermillion, K.L., Lidberg, K.A., and Gammill, L.S. (2014). Expression of actin-binding proteins and requirement for actin-depolymerizing factor in chick neural crest cells. *Dev. Dyn.* 243, 730–738.
 67. Ernst, J., and Kellis, M. (2012). ChromHMM: automating chromatin-state discovery and characterization. *Nat. Methods* 9, 215–216.
 68. Richardson, R.J., Hammond, N.L., Coulombe, P.A., Saloranta, C., Nousiainen, H.O., Salonen, R., Berry, A., Hanley, N., Headon, D., Karikoski, R., and Dixon, M.J. (2014). Periderm prevents pathological epithelial adhesions during embryogenesis. *J. Clin. Invest.* 124, 3891–3900.
 69. Fraser, H.B., Lam, L.L., Neumann, S.M., and Kobor, M.S. (2012). Population-specificity of human DNA methylation. *Genome Biol.* 13, R8.

70. Liu, J., Hutchison, K., Perrone-Bizzozero, N., Morgan, M., Sui, J., and Calhoun, V. (2010). Identification of genetic and epigenetic marks involved in population structure. *PLoS ONE* *5*, e13209.
71. Butali, A., Mossey, P.A., Adeyemo, W.L., Eshete, M.A., Gowans, L.J.J., Busch, T.D., Jain, D., Yu, W., Huan, L., Laurie, C.A., et al. (2019). Genomic analyses in African populations identify novel risk loci for cleft palate. *Hum. Mol. Genet.* *28*, 1038–1051.
72. Mukhopadhyay, N., Bishop, M., Mortillo, M., Chopra, P., Hetmanski, J.B., Taub, M.A., Moreno, L.M., Valencia-Ramirez, L.C., Restrepo, C., Wehby, G.L., et al. (2020). Whole genome sequencing of orofacial cleft trios from the Gabriella Miller Kids First Pediatric Research Consortium identifies a new locus on chromosome 21. *Hum. Genet* *139*, 215–226.
73. Carlson, J.C., Anand, D., Butali, A., Buxo, C.J., Christensen, K., Deleyiannis, F., Hecht, J.T., Moreno, L.M., Orioli, I.M., Padilla, C., et al. (2019). A systematic genetic analysis and visualization of phenotypic heterogeneity among orofacial cleft GWAS signals. *Genet. Epidemiol.* *43*, 704–716.
74. Huang, L., Jia, Z., Shi, Y., Du, Q., Shi, J., Wang, Z., Mou, Y., Wang, Q., Zhang, B., Wang, Q., et al. (2019). Genetic factors define CPO and CLO subtypes of nonsyndromic orofacial cleft. *PLoS Genet.* *15*, e1008357.
75. Ray, A.K., Marazita, M.L., Pathak, R., Beever, C.L., Cooper, M.E., Goldstein, T., Shaw, D.F., and Field, L.L. (2004). TP63 mutation and clefting modifier genes in an EEC syndrome family. *Clin. Genet.* *66*, 217–222.
76. Liu, H., Busch, T., Eliason, S., Anand, D., Bullard, S., Gowans, L.J.J., Nidey, N., Petrin, A., Augustine-Akpan, E.A., Saadi, I., et al. (2017). Exome sequencing provides additional evidence for the involvement of ARHGAP29 in Mendelian orofacial clefting and extends the phenotypic spectrum to isolated cleft palate. *Birth Defects Res.* *109*, 27–37.
77. Savastano, C.P., Brito, L.A., Faria, Á.C., Setó-Salvia, N., Peskett, E., Musso, C.M., Alvizi, L., Ezquina, S.A.M., James, C., GOS-gene, et al. (2017). Impact of rare variants in ARHGAP29 to the etiology of oral clefts: role of loss-of-function vs missense variants. *Clin. Genet.* *91*, 683–689.
78. Mansouri, A. (1998). The role of Pax3 and Pax7 in development and cancer. *Crit. Rev. Oncog.* *9*, 141–149.
79. Bishop, M.R., Diaz Perez, K.K., Sun, M., Ho, S., Chopra, P., Mukhopadhyay, N., Hetmanski, J.B., Taub, M.A., Moreno-Urbe, L.M., Valencia-Ramirez, L.C., et al. (2020). Genome-wide Enrichment of De Novo Coding Mutations in Orofacial Cleft Trios. *Am. J. Hum. Genet.* *107*, 124–136.